Electron and hole addition energies in PbSe quantum dots

J. M. An, A. Franceschetti, and A. Zunger
National Renewable Energy Laboratory, Golden, Colorado 80401, USA
(Received 18 January 2007; revised manuscript received 30 March 2007; published 5 July 2007)

We calculate electron and hole addition energies of PbSe quantum dots using a pseudopotential configuration-interaction approach. We find that (i) the addition energies are nearly constant for the first eight carriers occupying the *S*-like shell. (ii) The charging sequence of the first eight carriers is non-Aufbau, but filling of the *P*-like single-particle states takes place only after the *S*-like states are filled. (iii) The charging spectrum shows bunching-up of all lines as the dielectric constant ε_{out} of the material surrounding the dot increases. At the same time, the addition energies are significantly reduced. (iv) The calculated optical gap shows a rather weak dependence on ε_{out}, reflecting a cancellation between electron-hole interaction energies and surface polarization self-energies.

DOI: 10.1103/PhysRevB.76.045401 PACS number(s): 73.21.La

I. INTRODUCTION

PbSe quantum dots have been the subject of intense research in recent years, primarily because of efficient carrier multiplication rates[1,2] and relatively slow intraband relaxation rates.[3–5] In this paper, we focus on another unique property of PbSe quantum dots: the high multiplicity of the band-edge states, and its consequence on dot charging. In *bulk* PbSe,[6] both the valence-band maximum (VBM) and the conduction-band minimum (CBM) are located at the *L* point of the fcc Brillouin zone, and hence are fourfold degenerate (eightfold degenerate including Kramer's degeneracy), on account of the fourfold degeneracy of the *L* valleys. Correspondingly, in PbSe *quantum dots*, the first, *S*-like electron and hole confined states are eightfold degenerate. This degeneracy is split (by $4-7$ meV in a dot of radius $R=30.6$ Å, and by $16-35$ meV in a dot of $R=15.3$ Å) by intervalley couplings induced by the lack of translational symmetry.[7] The manifold of *S*-like electron states is separated from the next group of *P*-like states by a few hundred meV, whereas for the holes the *S*-*P* separation is a few tens of meV, as obtained by recent pseudopotential calculations[7,8] and by scanning tunneling measurements.[9] Because of the near-degeneracy of the band-edge *S*-like states, up to eight electrons or eight holes can be injected into these low-lying states. In this work, we study theoretically such charging effects.

Depending on the relative rates of carrier injection into the dot and carrier escape from the dot, one might be either in "accumulation mode"[10] (the *N*th injected carrier encounters $N-1$ pre-existing carriers) or in "tunneling mode"[10] (the dot has but one carrier at a time). In accumulation mode, the charging energy $\mu(N)$ is the energy required to add a carrier to the dot that is already loaded with $N-1$ carriers[11]:

$$\mu(N) = E(N) - E(N-1), \tag{1}$$

where $E(N)$ is the ground-state total energy of the *N*-carrier dot. The addition energy $\Delta(N,N-1)$ is the difference between the charging energy of the *N*th carrier and that of the $N-1$ carrier:

$$\Delta(N,N-1) = \mu(N) - \mu(N-1) = E(N) - 2E(N-1) + E(N-2). \tag{2}$$

Measurements of charging energies and addition energies by resonant tunneling spectroscopy were previously reported for colloidal nanocrystals such as InAs,[12] CdSe,[10] and ZnO.[13–15] Analysis of such measurements affords determination of the single-particle energy levels and the Coulomb repulsion energies between carriers.

In this work, we calculate electron and hole addition energies in PbSe quantum dots ($Pb_{260}Se_{249}$ and $Pb_{2046}Se_{2117}$), using a pseudopotential configuration-interaction approach. We find that (i) the addition energies are nearly constant for the first eight carriers occupying the *S*-like shell, (ii) the charging sequence of the first eight carriers is non-Aufbau, but filling of the *P*-like single-particle states takes place after the *S*-like states are completely filled, (iii) the charging spectrum shows bunching-up of all lines as the dielectric constant ε_{out} of the medium increases. At the same time, the addition energies are significantly reduced. (iv) The calculated optical gap shows a rather weak dependence on ε_{out}, reflecting a cancellation between the electron-hole interaction energies and the surface polarization self-energies.

II. BASIC PHYSICAL CONTRIBUTIONS TO THE ADDITION ENERGIES

A. *N*-particle total energy and its three contributions

The many-body total energy $E(N)$ of a dot containing *N* carriers can be calculated directly using the configuration interaction (CI) method[16] (see below), but it is instructive to separate it into its components, namely the first-order perturbation-theory energy $E_{PT}(N)$ and the correlation energy $E_{corr}(N)$. In turn, $E_{PT}(N)$ can be decomposed into a dot-intrinsic part $E_{PT}^{int}(N)$ and a surface-polarization part $E_{PT}^{pol}(N)$, so that

$$E(N) = E_{PT}^{int}(N) + E_{PT}^{pol}(N) + E_{corr}(N). \tag{3}$$

The three contributions to the total energy are discussed in the following.

The term $E_{PT}^{int}(N)$ is given by

$$E_{\mathrm{PT}}^{\mathrm{int}}(N) = \sum_{i}^{N} \varepsilon_i^0 + \frac{1}{2}\sum_{i,j}^{N} [U_{i,j;i,j}^{\mathrm{int}} - U_{i,j;j,i}^{\mathrm{int}}], \tag{4}$$

where ε_i^0 are the single-particle energies, $U_{i,j;i,j}^{\mathrm{int}}$ ($U_{i,j;j,i}^{\mathrm{int}}$) are the Coulomb direct (exchange) integrals, the subscripts i,j,k,l denote the collective index of orbital and spin states, and the sum runs over the occupied states. The general form of the Coulomb and exchange integrals $U_{i,j;k,l}^{\mathrm{int}}$ is

$$U_{i,j;k,l}^{\mathrm{int}} = \sum_{\sigma} \int \psi_i^*(\mathbf{r},\sigma)\psi_k(\mathbf{r},\sigma)\Phi_{j,l}^{\mathrm{int}}(\mathbf{r})d\mathbf{r}, \tag{5}$$

where $\{\psi_i(\mathbf{r},\sigma)\}$ are the single-particle wave functions (which depend on the spatial variable $\mathbf{r}$ and the spin variable σ), and $\Phi_{j,l}^{\mathrm{int}}(\mathbf{r})$ is the solution of the Poisson equation

$$\varepsilon(\mathbf{r})\nabla^2\Phi_{j,l}^{\mathrm{int}}(\mathbf{r}) = -4\pi e^2 \sum_{\sigma} \psi_j^*(\mathbf{r},\sigma)\psi_l(\mathbf{r},\sigma). \tag{6}$$

Here $\varepsilon(\mathbf{r})$ is the *macroscopic*, position-dependent dielectric constant.

The surface-polarization energy $E_{\mathrm{PT}}^{\mathrm{pol}}(N)$, due to the dielectric constant mismatch between the quantum dot and its surrounding material, is

$$E_{\mathrm{PT}}^{\mathrm{pol}}(N) = \sum_{i}^{N} \Sigma_i^{\mathrm{pol}} + \frac{1}{2}\sum_{i,j}^{N} [U_{i,j;i,j}^{\mathrm{pol}} - U_{i,j;j,i}^{\mathrm{pol}}], \tag{7}$$

where Σ_i^{pol} is the surface-polarization self-energy of a carrier in the single-particle state i, and $U_{i,j;i,j}^{\mathrm{pol}}$ ($U_{i,j;j,i}^{\mathrm{pol}}$) are the Coulomb direct (exchange) integrals arising from the interaction of one carrier with the image charge of other carriers across the dielectric discontinuity at the dot surface. The surface polarization self-energy is given in first-order perturbation theory by

$$\Sigma_i^{\mathrm{pol}} = \sum_{\sigma} \int |\psi_i(\mathbf{r},\sigma)|^2 \Sigma(\mathbf{r})d\mathbf{r}, \tag{8}$$

where $\Sigma(\mathbf{r})$ is the surface polarization potential

$$\Sigma(\mathbf{r}) = \frac{1}{2}\lim_{r'\to r}\{W_{\mathrm{dot}}(\mathbf{r},\mathbf{r}') - W_{\mathrm{bulk}}(\mathbf{r},\mathbf{r}')\}. \tag{9}$$

Here $W_{\mathrm{dot}}(\mathbf{r},\mathbf{r}')$ is the screened Coulomb potential of the quantum dot at point $\mathbf{r}$ due to a point charge located at $\mathbf{r}'$, and $W_{\mathrm{bulk}}(\mathbf{r},\mathbf{r}')$ is the same quantity in the corresponding bulk system.[17] Recently, Wang[18] showed that, under certain approximations, the quasiparticle GW equation for quantum dots can be simplified to an effective Schrödinger equation containing $\Sigma(\mathbf{r})$ as an external potential. Thus the quasiparticle energies can be written as $\varepsilon_i^{\mathrm{qp}} = \varepsilon_i^0 + \Sigma_i^{\mathrm{pol}}$. The surface polarization integrals $U_{i,j;k,l}^{\mathrm{pol}}$ of Eq. (7) are given by

$$U_{i,j;k,l}^{\mathrm{pol}} = \sum_{\sigma} \int \psi_i^*(\mathbf{r},\sigma)\psi_k(\mathbf{r},\sigma)\Phi_{j,l}^{\mathrm{pol}}(\mathbf{r})d\mathbf{r}, \tag{10}$$

where $\Phi_{j,l}^{\mathrm{pol}}(\mathbf{r})$ is the solution of the generalized Poisson equation,

$$\nabla\cdot\varepsilon(\mathbf{r})\nabla[\Phi_{j,l}^{\mathrm{int}}(\mathbf{r}) + \Phi_{j,l}^{\mathrm{pol}}(\mathbf{r})] = -4\pi e^2 \sum_{\sigma} \psi_j^*(\mathbf{r},\sigma)\psi_l(\mathbf{r},\sigma). \tag{11}$$

Finally, the correlation energy E_{corr} is defined in the CI approach as the residual effect that is obtained as a consequence of configuration mixing beyond the first-order approximation. Given the set of single-particle energies ε_i^0, the surface polarization self-energies $\{\Sigma_i^{\mathrm{pol}}\}$, and the set of Coulomb integrals $J_{i,j;k,l} = U_{i,j;k,l}^{\mathrm{int}} + U_{i,j;k,l}^{\mathrm{pol}}$, the many-body CI Hamiltonian is given in second-quantization form by

$$H = \sum_{i} [\varepsilon_i^0 + \Sigma_i^{\mathrm{pol}}]\hat{c}_i^\dagger\hat{c}_i + \frac{1}{2}\sum_{ijkl} J_{i,j;k,l}\hat{c}_i^\dagger\hat{c}_j^\dagger\hat{c}_l\hat{c}_k. \tag{12}$$

The diagonalization of the CI Hamiltonian (12) yields the many-particle energies and wave functions.

B. Charging energies and addition energies

Following the decomposition of the total energy into three contributions [Eq. (3)], we can write the charging energies $\mu(N)$ as

$$\mu(N) = \mu_{\mathrm{PT}}^{\mathrm{int}}(N) + \mu_{\mathrm{PT}}^{\mathrm{pol}}(N) + \mu_{\mathrm{corr}}(N), \tag{13}$$

where

$$\mu_{\mathrm{PT}}^{\mathrm{int}}(N) = \varepsilon_N^0 + \sum_{i=1}^{N-1} (U_{i,N;i,N}^{\mathrm{int}} - U_{i,N;N,i}^{\mathrm{int}}), \tag{14}$$

$$\mu_{\mathrm{PT}}^{\mathrm{pol}}(N) = \Sigma_N^{\mathrm{pol}} + \sum_{i=1}^{N-1} (U_{i,N;i,N}^{\mathrm{pol}} - U_{i,N;N,i}^{\mathrm{pol}}), \tag{15}$$

and $\mu_{\mathrm{corr}}(N)$ is the effect of configuration mixing.

Similarly, the contributions to the addition energies $\Delta(N,N-1)$ are

$$\Delta(N,N-1) = \Delta_{\mathrm{PT}}^{\mathrm{int}}(N,N-1) + \Delta_{\mathrm{PT}}^{\mathrm{pol}}(N,N-1) + \Delta_{\mathrm{corr}}(N,N-1), \tag{16}$$

where

$$\Delta_{\mathrm{PT}}^{\mathrm{int}}(N,N-1) = [\varepsilon_N^0 - \varepsilon_{N-1}^0] + \sum_{i=1}^{N-1} [U_{i,N;i,N}^{\mathrm{int}} - U_{i,N;N,i}^{\mathrm{int}}] - \sum_{i=1}^{N-2} [U_{i,N-1;i,N-1}^{\mathrm{int}} - U_{i,N-1;N-1,i}^{\mathrm{int}}], \tag{17}$$

$$\Delta_{\mathrm{PT}}^{\mathrm{pol}}(N,N-1) = [\Sigma_N^{\mathrm{pol}} - \Sigma_{N-1}^{\mathrm{pol}}] + \sum_{i=1}^{N-1} [U_{i,N;i,N}^{\mathrm{pol}} - U_{i,N;N,i}^{\mathrm{pol}}] - \sum_{i=1}^{N-2} [U_{i,N-1;i,N-1}^{\mathrm{pol}} - U_{i,N-1;N-1,i}^{\mathrm{pol}}], \tag{18}$$

and $\Delta_{\mathrm{corr}}(N,N-1)$ is the additional effect arising from the configuration mixing as mentioned above.

C. Quasiparticle band gap

The quasiparticle gap $\varepsilon_{\rm gap}^{\rm qp}$ is the minimum energy necessary to remove an electron from the valence band of one dot and place it into the conduction band of another dot at infinite distance from the first dot. Thus the electron and the hole do not interact. In first-order perturbation theory, the quasiparticle gap is given by

$$\varepsilon_{\rm gap}^{\rm qp} = [\varepsilon_{e1}^0 - \varepsilon_{h1}^0] + [\Sigma_{e1}^{\rm pol} + \Sigma_{h1}^{\rm pol}]. \tag{19}$$

The optical gap $\varepsilon_{\rm gap}^{\rm opt}$ is

$$\begin{aligned}\varepsilon_{\rm gap}^{\rm opt} &= \varepsilon_{\rm gap}^{\rm qp} - J_{h1,e1;h1,e1} \\ &= [\varepsilon_{e1}^0 - \varepsilon_{h1}^0] + [\Sigma_{e1}^{\rm pol} + \Sigma_{h1}^{\rm pol}] - J_{h1,e1;h1,e1},\end{aligned} \tag{20}$$

and includes direct electron-hole Coulomb attraction.

III. METHOD OF CALCULATIONS

The calculation of $E(N)$ requires solving the many-body CI Hamiltonian of Eq. (12). The single-particle energies and wave functions are obtained by solving the effective Schrödinger equation

$$\left[-\frac{1}{2}\nabla^2 + V(\mathbf{r}) + V_{\rm SO}\right]\psi_i(\mathbf{r},\sigma) = \varepsilon_i^0 \psi_i(\mathbf{r},\sigma), \tag{21}$$

where the wave functions $\psi_i(\mathbf{r},\sigma)$ are expanded in a plane-wave basis set, and $V_{\rm SO}$ is the nonlocal spin-orbit operator. The local potential $V(\mathbf{r})$ is represented as a superposition of screened atomic pseudopotentials for atom species α at sites $\mathbf{R}_{n,\alpha}$,

$$V(\mathbf{r}) = \sum_{n,\alpha} v_\alpha(\mathbf{r} - \mathbf{R}_{n,\alpha}). \tag{22}$$

The atomic pseudopotentials v_α are fitted to bulk transition energies, effective masses, and deformation potentials.[7]

The calculation of the surface polarization self-energies $\Sigma_i^{\rm pol}$ [Eqs. (8) and (9)] requires solving the generalized Poisson equation for a point-charge density distribution:[11,18]

$$\nabla \cdot \varepsilon(\mathbf{r}) \nabla W_{\rm dot}(\mathbf{r},\mathbf{r}') = -4\pi e^2 \delta(\mathbf{r} - \mathbf{r}'), \tag{23}$$

$$\varepsilon(\mathbf{r})\nabla^2 W_{\rm bulk}(\mathbf{r},\mathbf{r}') = -4\pi e^2 \delta(\mathbf{r} - \mathbf{r}'). \tag{24}$$

The macroscopic dielectric function $\varepsilon(\mathbf{r})$ is calculated as $1/\varepsilon(\mathbf{r}) = 1/\varepsilon_{\rm out} + [1/\varepsilon_{\rm in} - 1/\varepsilon_{\rm out}]m(\mathbf{r})$, where $\varepsilon_{\rm in}$ and $\varepsilon_{\rm out}$ are the dielectric constants inside and outside the quantum dot, respectively. The mask function $m(\mathbf{r})$ decays sinusoidally from 1 to 0 in a ~2-Å-thick transition region around the dot surface. Recent first-principles calculations[19,20] have shown that $\varepsilon(\mathbf{r})$ converges rapidly to the value of the bulk dielectric constant as the interior of the dot is approached. Furthermore, since the motion of the electrons is much faster than that of the ions, the ionic contribution to $\varepsilon_{\rm in}$ is small, and will be neglected here. We will also neglect the small change in $\varepsilon_{\rm in}$ upon electron and/or hole charging, since the added carriers represent only a small fraction of the total number of electrons in the quantum dot. Therefore for $\varepsilon_{\rm in}$ we use the high-frequency dielectric constant of bulk PbSe ($\varepsilon_{\rm in}$=22.9).

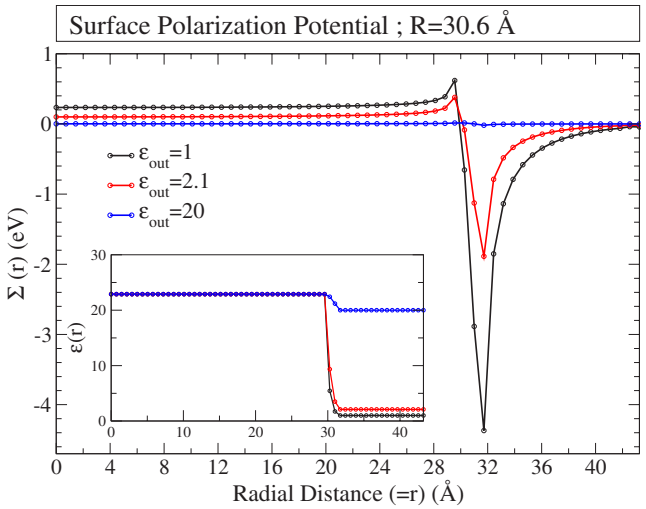

FIG. 1. (Color online) The surface polarization potential $\Sigma(r)$ of a 30.6-Å-radius PbSe quantum dot is shown as a function of the radial distance r from the center of the dot, for three different values of the macroscopic dielectric constant of the surrounding medium ($\varepsilon_{\rm out}$=1, 2.1, 20). The inset shows the corresponding dielectric function profile $\varepsilon(r)$. Circles denote the calculated values, to which the solid curves are fitted.

The value of $\varepsilon_{\rm out}$ is varied to simulate different dielectric environments. The δ functions in Eqs. (23) and (24) are approximated by a Gaussian of width 0.8 Å centered at position $\mathbf{r}'$. The Poisson Eqs. (23) and (24) are solved numerically by discretizing the gradient operator on a real-space uniform grid.[11] The boundary conditions are obtained by expanding the electrostatic potential in a multipole series, and the resulting linear system is solved using a conjugate-gradients algorithm.[11] Similarly, the Coulomb integrals $\{J_{i,j;k,l}\}$ of Eq. (12) are calculated by solving the generalized Poisson equation of Eq. (11).

The ground-state energy of the N-carrier dot is obtained by diagonalizing the many-body Hamiltonian of Eq. (12) in the configuration space constructed from the first eight hole or electron states:

$$E(N) = \langle \Psi_N | H | \Psi_N \rangle, \tag{25}$$

where Ψ_N is the ground-state many-body wave function of the N-particle system.

IV. RESULTS

A. Surface polarization self-energy

The surface polarization potential $\Sigma(\mathbf{r})$ of Eq. (9) was calculated at 30 real-space grid points for the 15.3-Å-radius dot and 60 points for the 30.6-Å-radius dot along the [110] axis of the fcc supercell, and the results were interpolated throughout the whole supercell. As an example, Fig. 1 shows the calculated values of $\Sigma(\mathbf{r})$ for the R=30.6-Å dot with different dielectric function profiles (corresponding to $\varepsilon_{\rm in}$ =22.9 and $\varepsilon_{\rm out}$=1, 2.1, and 20) along the [110] axis. The sharp change of $\Sigma(\mathbf{r})$ near the dot boundary is due to the

TABLE I. Surface polarization self-energy Σ_i^{pol} (in meV) of a carrier occupying the ith single-particle electron (e_i) or hole (h_i) level for three different values of the macroscopic dielectric constant of the surrounding medium, ε_{out}.

Radius (Å)	ε_{out}	e_1	e_2	e_3	e_4	h_1	h_2	h_3	h_4
15.3 Å	1	374.3	375.5	340.4	423.7	371.1	370.8	369.4	456.9
	2.1	198.7	199.2	182.2	216.4	193.4	193.3	193.1	233.6
	20	5.3	5.3	5.0	5.1	4.9	4.9	4.9	5.5
30.6 Å	1	209.6	226.4	220.9	222.3	213.4	229.6	229.6	231.3
	2.1	104.7	111.2	108.4	109.0	105.3	110.9	110.9	111.6
	20	2.8	2.8	2.8	2.8	2.7	2.7	2.7	2.7

dielectric function transition from ε_{in} to ε_{out}. A similar behavior of $\Sigma(\mathbf{r})$ is also observed for the 15.3-Å dot, but the value of $\Sigma(\mathbf{r})$ inside the dot is larger than that for the 30.6-Å-radius dot, because of the closer proximity of the dot surface.

Table I summarizes our calculated surface polarization self-energies Σ_i^{pol} for several band-edge electron (e_i) and hole (h_i) single-particle states, and for a few different dielectric function profiles. The effect of ε_{out} on Σ_i^{pol} is strong, as exemplified by the e_1 state of the $R=15.3$-Å dot whose surface polarization energy decreases from ~374 meV for $\varepsilon_{\text{out}}=1$ to ~5 meV for $\varepsilon_{\text{out}}=20$. For a given ε_{out}, the value of Σ_i^{pol} depends rather weakly upon the single-particle state. However, some single-particle states, such as e_4 and h_4, have considerably larger Σ_i^{pol} (by as much as 87 meV for $\varepsilon_{\text{out}}=1$) than the other states. In general, states that have a relatively large weight just outside the dot boundary have smaller Σ_i^{pol} than states that are more localized inside the dot, because $\Sigma(\mathbf{r})$ becomes negative outside the dot boundary (Fig. 1). This Σ_i^{pol} difference among single-particle states is sufficiently large to determine a change in the ordering of the levels in the single-particle energy ladder.

B. Charge distribution of the injected carriers

It is interesting to consider the spatial distribution of the loaded carriers. In a classical electrostatic model where the carriers are described by point charges that are free to move inside a dielectric sphere,[21] Coulomb repulsion leads to localization of the injected carriers near the surface of the quantum dot. In our quantum-mechanical calculations, carrier localization is determined by the spatial localization of the single-particle wave functions and by the mixing of different configurations via configuration interaction. Because of the relatively large splitting between S and P levels and the large dielectric constant of PbSe (which effectively screens carrier-carrier interactions), configuration mixing beyond the S-like manifold is small. In the absence of surface states near the band edges, the first eight injected carriers will occupy S-like, quantum-confined states, and their charge distribution will be largely localized in the dot interior. However, the inorganic ligand shell surrounding the PbSe quantum dots can hardly passivate all surface anions and cations, resulting in localized surface states. In that case, part of the injected carriers will reside at the surface of the quantum dots.

C. Charging spectrum and addition energies

Figures 2 and 3 show the charging spectrum and the addition energies $\Delta(N,N-1)$ obtained by diagonalizing the CI many-body Hamiltonian for $\varepsilon_{\text{out}}=1,2.1,20$. Figures 2(a) and 3(a) show the charging spectra of the $R=15.3$-Å and $R=30.6$-Å dots, respectively. The position of the peaks corresponds to the calculated charging energies, while the intensity of the peaks is normalized to unity. We see that as the dot size increases, the span of the charging energies corresponding to loading eight electrons or eight holes decreases considerably. Furthermore, as the dielectric constant ε_{out} of the environment increases, the charging spectrum shows bunching of the peaks, because the separation between the charging peaks becomes smaller as ε_{out} increases. In Figs. 2(a) and 3(a) $\mu=0$ is the chemical potential of the electron reservoir. Thus for $\mu<0$ electrons are attracted to the quantum dot, while for $\mu>0$ electrons are repelled. We see from the charging spectra of Figs. 2(a) and 3(a) that only a limited number of electrons (corresponding to the peaks with $\mu\leq 0$) can be loaded into the quantum dot. The number of electrons that can be injected into the dot becomes smaller as the dielectric constant of the environment decreases. For example, in the case of the $R=15.3$-Å dot, up to six electrons can be loaded into the dot if $\varepsilon_{\text{out}}=2.1$, but only three electrons if $\varepsilon_{\text{out}}=1$ [Fig. 2(a)].

Figures 2(b) and 3(b) show that the addition energies depend only weakly on the number N of carriers within the S shell. This behavior of $\Delta(N,N-1)$ can be recovered by reformulating Eq. (16) under the following approximations: (i) The single-particle energy levels $(\varepsilon_i^0+\Sigma_i^{\text{pol}})$ are the same for the first few single-particle states, (ii) the correlation energy Δ_{corr} is negligible compared to the other terms, and (iii) the total Coulomb repulsion $(J_{i,j;i,j}\equiv J)$ between carriers is almost constant (i.e., independent of i and j), and is much larger than the exchange interaction $J_{i,j;j,i}$. With the approximation (ii), Eq. (16) reduces to

$$\Delta(N,N-1)=[\varepsilon_N^0-\varepsilon_{N-1}^0]+[\Sigma_N^{\text{pol}}-\Sigma_{N-1}^{\text{pol}}]+\sum_i^{N-1}[J_{i,N;i,N}-J_{i,N;N,i}]-\sum_i^{N-2}[J_{i,N-1;i,N-1}-J_{i,N-1;N-1,i}]. \quad (26)$$

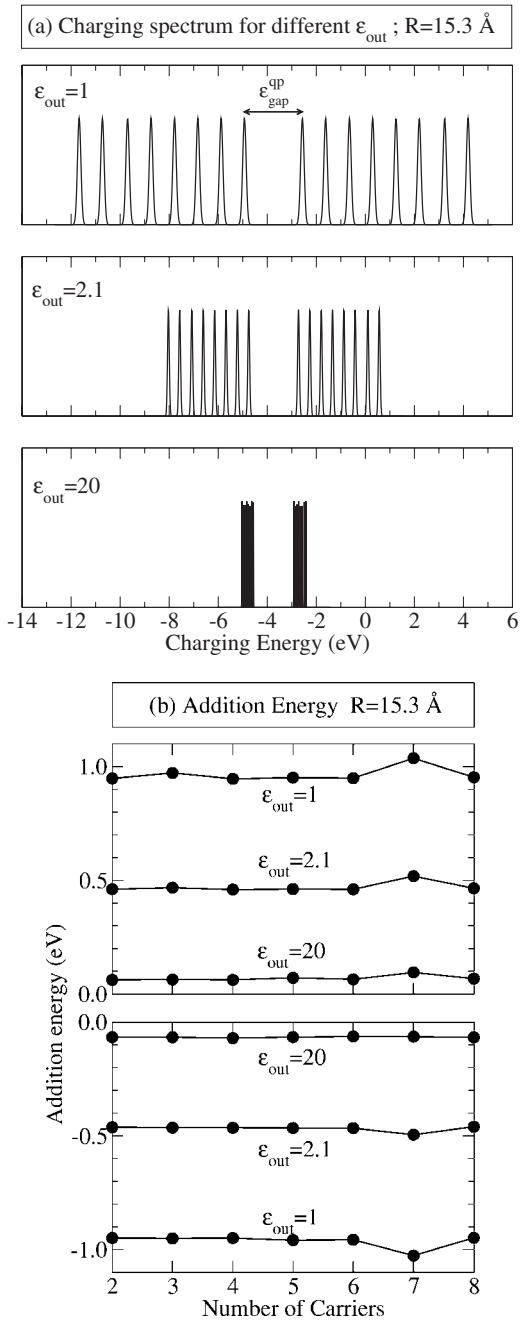

FIG. 2. Electron and hole charging energies (a) and addition energies (b) of a $R=15.3$-Å PbSe quantum dot, calculated for three values of the macroscopic dielectric constant of the surrounding medium ($\varepsilon_{\text{out}}=1,2.1,20$). For clarity purposes, in (b) the hole addition energies are indicated with a negative value.

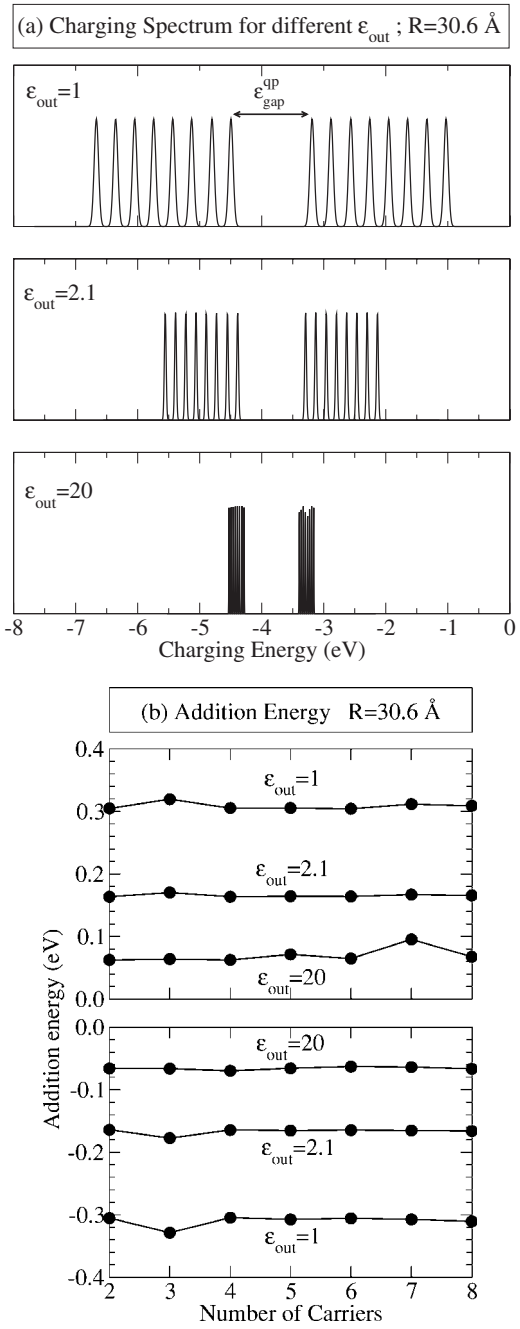

FIG. 3. Electron and hole charging energies (a) and addition energies (b) of a $R=30.6$-Å PbSe quantum dot, calculated for three values of the macroscopic dielectric constant of the surrounding medium ($\varepsilon_{\text{out}}=1,2.1,20$). For clarity purposes, in (b) the hole addition energies are indicated with a negative value.

The successive application of approximations (i) and (iii) leads to

$$\Delta(N,N-1)=J, \tag{27}$$

which describes the trend in the numerical results. Thus the value of $\Delta(N,N-1)$ can be interpreted as an indirect measure of the Coulomb repulsion between carriers, independent of N under the aforementioned approximations. When the small spacings between the quasiparticle energy levels are taken into account, however, $\Delta(N,N-1)$ is more pronounced for odd values of N, because each orbital level can be occupied by two carriers. The nearly constant value of $\Delta(N,N-1)$ as a function of N is characteristic of quantum dots where the near-edge states are highly degenerate. For example, in Si quantum dots, where the S-like conduction-band edge states originate from the six X valleys of bulk Si, up to 12 electrons can be loaded into the nearly degenerate S-like conduction

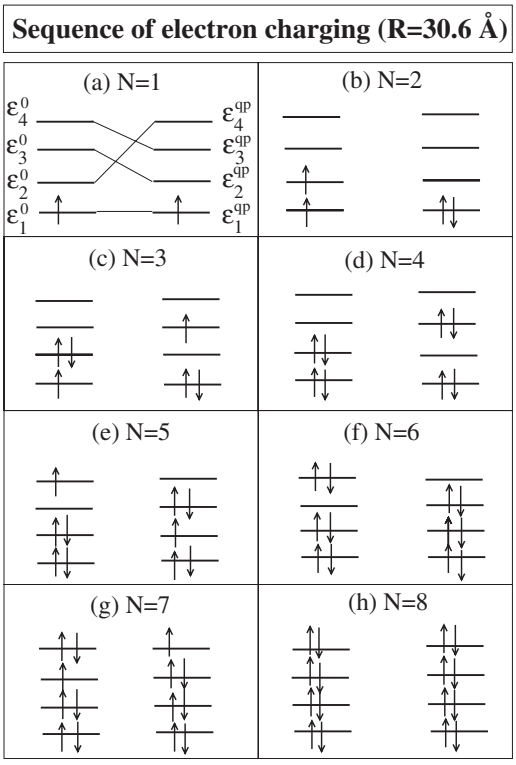

FIG. 4. Charging sequence of N electrons loaded into the $R=30.6$-Å PbSe dot. The left-hand side of each panel shows schematically the single-particle energy levels (ε_i^0), while the right-hand side shows the quasiparticle energy levels ($\varepsilon_i^{qp}=\varepsilon_i^0+\Sigma_i^{pol}$).

states, and therefore $\Delta(N,N-1)$ is nearly constant up to $N=12$ (Ref. 11).

D. Minimum-energy electronic configuration for different charge states

To determine the ground-state configuration of a system of N electrons (or N holes) in a quantum dot, we compute the ground-state total energy $E(N)$ using the basis set of configurations constructed from the first eight hole states and the first eight electron states. We then examine the ground-state CI wave functions $\Psi(1),\ldots,\Psi(8)$, and investigate in what order the carriers occupy the single-particle energy levels ε_i^0 or the quasiparticle energy levels $\varepsilon_i^{qp}=\varepsilon_i^0+\Sigma_i^{pol}$. This will determine whether or not the CI ground state for N carriers corresponds to occupying ε_i^0 (or ε_i^{qp}) in increasing order (Aufbau principle). Figure 4 shows the charging sequence of N electrons occupying the single-particle levels ε_i^0 and the quasiparticle levels ε_i^{qp} for the $R=30.6$-Å dot. Note that the inclusion of Σ_i^{pol} changes the sequence of the quasiparticle energy levels compared to the sequence of the single-particle levels. For example, the energy of the level e_2 becomes higher than that of e_3 or e_4 after the polarization self energies are included [Fig. 4(a)]. Whether the occupation sequence is determined with reference to the single-particle levels or the quasiparticle levels, there are many instances where the Aufbau principle is violated, due to the near-degeneracy of the first eight hole states and the first eight electron states. Violations of the Aufbau occupation sequence have also been observed for other dot sizes and for different values of the dielectric constant ε_{out}.

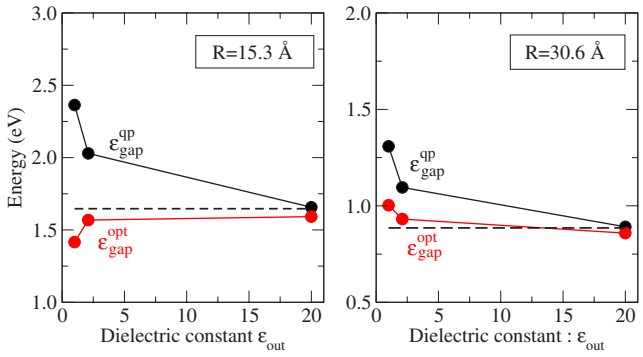

FIG. 5. (Color online) Calculated quasiparticle gap ε_{gap}^{qp} and optical gap ε_{gap}^{opt} of PbSe dots of $R=15.3$ Å and 30.6 Å, as a function of the dielectric constant of surrounding material, ε_{out}. The single-particle energy gap ε_{gap}^0 is indicated by a dashed line.

We find that the added carriers never fill the higher-energy manifold of P-like states before the eight S-like states are completely filled. This is due to the relatively large S-P splitting ($\Delta_{SP}=72$ meV for hole levels and $\Delta_{SP}=127$ meV for electron levels for the $R=30.6$-Å dot). Wehrenberg and Guyot-Sionnest[22] recently reported injection of electron and holes into PbSe nanocrystals, and measured the ensuing changes in the interband and intraband optical-absorption spectra. They found that the first two interband absorption peaks were both bleached when electrons were loaded into the quantum dots. Since the first eight injected electrons occupy S-like levels [see also Fig. 4(h)], the authors concluded that the first two interband absorption peaks must both involve transitions into the S-like electron states.[22] Previous atomistic pseudopotential calculations[7] have shown instead that the first two interband absorption peaks originate from the allowed S_h-S_e and P_h-P_e transitions, respectively, and that the second absorption peak does not involve S-like electron states. The apparent contradiction between experiment[22] and theory[7] can be resolved by noting that not all of the injected carriers necessarily reside in dot-interior, quantum-confined states. Indeed, it is likely that some of the injected carriers occupy localized states near the surface of the quantum dot. These surface charges induce a Stark shift of all absorption peaks, as well as a reduction in the intensity of the allowed transitions, consistent with the experimental results of Ref. 22. This will be discussed in a forthcoming publication.[23]

E. Quasiparticle gap

Figure 5 shows the calculated quasiparticle gap ε_{gap}^{qp} [Eq. (19)], the optical gap ε_{gap}^{opt} [Eq. (20)], and the single-particle gap $\varepsilon_{e1}^0-\varepsilon_{h1}^0$. Not surprisingly, $\varepsilon_{gap}^{qp}>\varepsilon_{gap}^{opt}$. We see from Fig. 5 that the quasiparticle gap ε_{gap}^{qp} depends rather strongly on the dielectric constant ε_{out} of the medium, because of the terms Σ_i^{pol} appearing in Eq. (19). However, the optical gap has but a weak dependence on ε_{out}, because of the near-cancellation

of $\Sigma_{e1}^{\mathrm{pol}}+\Sigma_{h1}^{\mathrm{pol}}$ against $J_{h1,e1;h1,e1}$ in Eq. (20). As a result, $\varepsilon_{\mathrm{gap}}^{\mathrm{opt}}$ is close to the single-particle gap $\varepsilon_{e1}^{0}-\varepsilon_{h1}^{0}$, and shows a rather weak dependence on $\varepsilon_{\mathrm{out}}$. This cancellation is not particular to PbSe dots, and a similarly weak dependence of $\varepsilon_{\mathrm{gap}}^{\mathrm{opt}}$ on $\varepsilon_{\mathrm{out}}$ was previously reported for InAs, InP, and Si quantum dots.[11]

V. SUMMARY

In summary, we have calculated the electron and hole addition energies of PbSe quantum dots using a pseudopotential configuration-interaction approach. We have decomposed the addition energies into physically distinct contributions. This has revealed peculiar features of the charging spectrum of PbSe quantum dots: (i) The addition energies are nearly constant for the first eight carriers occupying quantum-confined *S*-like states. (ii) While the charging sequence of the first eight carriers is non-Aufbau, filling of the *P*-like single-particle states takes place only after the *S*-like states are completely filled. We also found general features of the charging spectrum that are not specific to PbSe dots. (iii) The charging spectrum shows bunching-up of all lines as the dielectric constant $\varepsilon_{\mathrm{out}}$ of the material surrounding the dot increases. (iv) The calculated optical gap shows a rather weak dependence on $\varepsilon_{\mathrm{out}}$, reflecting a cancellation between electron-hole Coulomb interaction energies and surface polarization self-energies.

ACKNOWLEDGMENTS

This work was funded by the U.S. Department of Energy, Office of Science, Basic Energy Science, Materials Sciences and Engineering, under Contract No. DE-AC36-99GO10337 to NREL.

[1] R. D. Schaller and V. I. Klimov, Phys. Rev. Lett. **92**, 186601 (2004).
[2] R. J. Ellingson, M. C. Beard, J. C. Johnson, P. Yu, O. I. Micic, A. J. Nozik, A. Shabaev, and A. L. Efros, Nano Lett. **5**, 865 (2005).
[3] J. M. Harbold, H. Du, T. D. Krauss, K.-S. Cho, C. B. Murray, and F. W. Wise, Phys. Rev. B **72**, 195312 (2005).
[4] B. L. Wehrenberg, C. Wang, and P. Guyot-Sionnest, J. Phys. Chem. B **106**, 10634 (2002).
[5] R. D. Schaller, J. M. Pietryga, S. V. Goupalov, M. A. Petruska, S. A. Ivanov, and V. I. Klimov, Phys. Rev. Lett. **95**, 196401 (2005).
[6] S. H. Wei and A. Zunger, Phys. Rev. B **55**, 13605 (1997).
[7] J. M. An, A. Franceschetti, S. V. Dudiy, and A. Zunger, Nano Lett. **6**, 2728 (2006).
[8] A. Franceschetti, J. M. An, and A. Zunger, Nano Lett. **6**, 2191 (2006).
[9] P. Liljeroth, P. A. Z. van Emmichoven, S. G. Hickey, H. Weller, B. Grandidier, G. Allan, and D. Vanmaekelbergh, Phys. Rev. Lett. **95**, 086801 (2005).
[10] E. P. A. M. Bakkers, Z. Hens, A. Zunger, A. Franceschetti, L. P. Kouwenhoven, L. Gurevich, and D. Vanmaekelbergh, Nano Lett. **1**, 551 (2001).
[11] A. Franceschetti and A. Zunger, Phys. Rev. B **62**, 2614 (2000).
[12] U. Banin, Y. Cao, D. Katz, and O. Millo, Nature (London) **400**, 542 (1999).
[13] A. L. Roest, J. J. Kelly, D. Vanmaekelbergh, and E. A. Meulenkamp, Phys. Rev. Lett. **89**, 036801 (2002).
[14] A. Germeau, A. L. Roest, D. Vanmaekelbergh, G. Allan, C. Delerue, and E. A. Meulenkamp, Phys. Rev. Lett. **90**, 097401 (2003).
[15] M. Shim and P. Guyot-Sionnest, Phys. Rev. Lett. **91**, 169703 (2003).
[16] A. Franceschetti, H. Fu, L. W. Wang, and A. Zunger, Phys. Rev. B **60**, 1819 (1999).
[17] L. E. Brus, J. Chem. Phys. **79**, 5566 (1983); **80**, 4403 (1984).
[18] L.-W. Wang, J. Phys. Chem. B **109**, 23330 (2005).
[19] X. Cartoixa and L.-W. Wang, Phys. Rev. Lett. **94**, 236804 (2005).
[20] A. Franceschetti and M. C. Troparevsky, Phys. Rev. B **72**, 165311 (2005).
[21] J. W. Zhu, T. LaFave, and R. Tsu, Microelectron. J. **37**, 1293 (2006).
[22] B. L. Wehrenberg and P. Guyot-Sionnest, J. Am. Chem. Soc. **125**, 7806 (2003).
[23] J. M. An, A. Franceschetti, and A. Zunger (unpublished).